

Micro- and millimeter-wave spectra of five conformers of cysteamine and their interstellar search[★]

Wentao Song¹, Assimo Maris¹, Víctor M. Rivilla^{2,3}, Francesca Fortuna¹, Luca Evangelisti¹, Dingding Lv¹, Lucas Rodríguez-Almeida², Izaskun Jiménez-Serra², Jesús Martín-Pintado², and Sonia Melandri¹

¹ Department of Chemistry “Giacomo Ciamician”, University of Bologna, Via Selmi 2, Bologna, Italy
e-mail: sonia.melandri@unibo.it

² Centro de Astrobiología (CSIC-INTA), Ctra. de Ajalvir Km. 4, Torrejón de Ardoz, 28850 Madrid, Spain
e-mail: vrvilla@cab.inta-csic.es

³ INAF-Osservatorio Astrofisico di Arcetri, Florence, Italy

Received 20 December 2021 / Accepted 2 February 2022

ABSTRACT

Context. Cysteamine ($\text{NH}_2\text{CH}_2\text{CH}_2\text{SH}$), a molecule of potential astrobiological interest, has not yet been detected in the interstellar medium. Furthermore, the sulfur-substituted isomer of ethanolamine (or 2-aminoethanol) has been recently detected in the molecular cloud G+0.693–0.027.

Aims. In order to conduct a new interstellar search for cysteamine in the molecular cloud G+0.693–0.027, its pure rotational spectrum needs to be investigated in the laboratory.

Methods. A pulsed-jet Fourier transform microwave spectrometer and a Stark-modulated free-jet millimeter-wave absorption spectrometer were used to measure the purely rotational spectrum of cysteamine in the range of 6.5–18 GHz (46.12–16.66 mm) and 59.6–120.0 GHz (5.03–2.72 mm), respectively. We used a deep spectral line survey toward the molecular cloud G+0.693–0.027 obtained with the IRAM 30 m and Yebes 40 m radiotelescopes to search for cysteamine.

Results. We assigned 815 rotational transition lines of five conformers (gGt , gGg , $g'Gg$, $g'Gg'$, and $g'Gt$) to fit the rotational constants, quartic centrifugal distortion constants, and the ^{14}N nuclear quadrupole coupling constants. For four conformers (gGt , gGg , $g'Gg$, and $g'Gg'$), the ^{34}S isotopologs were observed, and for two of them (gGg and $g'Gg'$), the ^{13}C and ^{15}N isotopolog spectra were also detected; all in natural abundance. The five conformers of cysteamine were not detected toward the G+0.693–0.027 molecular cloud. We derived upper limits for their molecular abundances compared to molecular hydrogen of $<(0.2\text{--}1.3) \times 10^{-10}$. The relative abundances with respect to the oxygen counterpart ethanolamine, previously detected toward this cloud, are $\text{NH}_2\text{CH}_2\text{CH}_2\text{OH}/\text{NH}_2\text{CH}_2\text{CH}_2\text{SH} > 0.8\text{--}5.3$.

Key words. ISM: molecules – techniques: spectroscopic – methods: laboratory: molecular – molecular data – surveys – line: identification

1. Introduction

Sulfur-containing species are found in the interstellar medium (ISM), but their chemical evolution is not fully understood so far. Sulfur is abundant in the Solar System; it is present in the clouds of the four giant planets, for instance, in the atmosphere of Venus, and on several icy moons. In space, the abundances of sulfur-containing species are particularly sensitive to the physical and chemical changes, so that sulfur-bearing species have been used to probe the physical structure of star-forming regions (Lada et al. 1991; Plume et al. 1997) and to track the evolution of hot cores (Hatchell et al. 1998) and protostellar sources (Oya et al. 2019). For example, the ratios of SO_2/SO , $\text{SO}_2/\text{H}_2\text{S}$, and $\text{OCS}/\text{H}_2\text{S}$ are regarded as chemical clocks in these regions (Charnley 1997; Hatchell et al. 1998; Wakelam et al. 2011). However, recent theoretical and observational studies have shown that the situation is more complicated than previously thought. The abundance of sulfur in the gas phase in the diffuse ISM is comparable to that in the Solar System (Savage & Sembach 1996), but it is much lower in the cold ISM (Joseph et al. 1986;

Goicoechea et al. 2021; Laas & Caselli 2019). This difference may be caused by the accretion of sulfur on solid dust particles. However, the form of sulfur in these dust grains is still uncertain, so that further astronomical exploration is necessary.

Radio astronomy is recognized as one of the most effective techniques to search for interstellar molecules. By comparing the spectra of candidate molecules in the laboratory with the spectra observed in astronomical surveys, we can determine whether these molecules exist in interstellar space. Therefore, it is necessary to provide rotational spectra of candidates for astronomical detection. Radio astronomy has helped to detect several sulfur-containing molecules in the ISM in recent years: in particular, thiols, the sulfur analogs of alcohols. Methanethiol (or methyl mercaptan, CH_3SH) was detected in the Sagittarius B2 (Sgr B2) region of the center of our Galaxy (Linke et al. 1979; Gibb et al. 2000; Müller et al. 2016; Rodríguez-Almeida et al. 2021) and in the protostar IRAS 16293–2422 (Majumdar et al. 2016). Two groups reported to have detected several signs of ethanethiol ($\text{C}_2\text{H}_5\text{SH}$) in Sgr B2 (Müller et al. 2016) and Orion (Kolesníková et al. 2014). Most recently, Rodríguez-Almeida reported the first unambiguous detection of ethanethiol in the ISM, toward the G+0.603–0.027 molecular cloud (Rodríguez-Almeida et al. 2021). Moreover, several sulfur-containing species

[★] Data are only available at the CDS via anonymous ftp to [cdsarc.u-strasbg.fr](ftp://cdsarc.u-strasbg.fr) (130.79.128.5) or via <http://cdsarc.u-strasbg.fr/viz-bin/cat/J/A+A/661/A129>

have been observed in comets (Altwegg et al. 2017). Some recent efforts, both from spectroscopy and astronomical searches, to detect S-substitutes of other classes of compounds have also been reported. For instance, thioformic acid (HC(O)SH) was very recently detected in G+0.693-0.027. Its trans-isomer has an abundance of $\sim 1 \times 10^{-10}$ (Rodríguez-Almeida et al. 2021). Conversely, thioformamide (NH₂CHS), the counterpart of formamide (NH₂CHO), was characterized in the laboratory up to 660 GHz, and its transitions were searched for toward the hot cores Sgr B2(N1S) and Sgr B2(N2), but it was not detected (Motiyenko et al. 2020). The rotational spectrum of thioacetamide was recently analyzed in the 59.6–110.0 GHz frequency region (5.03–2.72 mm). Its emission was searched for in regions associated with star formation using the IRAM 30 m ASAI observations toward the prestellar core L1544 and the outflow shock L1157-B1. The molecule was not detected, but the study allowed placing constraints on the thioacetamide abundances (Maris et al. 2019; Remijan et al. 2022).

Regarding more complex molecules, as it is well known, amino acids are the basic unit of proteins and have an extremely important significance in astrobiology as they are considered the building blocks of life. A possible precursor for the formation of the simplest amino acids, glycine (C₂H₅NO₂) and alanine (C₃H₇NO₂), has been postulated to be ethanolamine (2-aminoethanol; NH₂CH₂CH₂OH), which is also considered the simplest phospholipid head group (Charnley et al. 2001; Courmier et al. 2005; Bossa et al. 2009; Duvernay et al. 2010). Sulfur is an important biogenic element and is a component of the amino-acid cysteine (C₃H₇NO₂S) found in terrestrial biological systems, therefore cysteamine (also known as 2-aminoethanethiol, mercaptamine or thioethanolamine; NH₂CH₂CH₂SH), which is the sulfur analog of ethanolamine, could have a potential astrobiological interest. Recently, Rivilla and coworkers observed ethanolamine in the molecular cloud G+0.693–0.027 (hereafter G+0.693), located in the Sgr B2 complex in the Galactic center (Rivilla et al. 2021b), thanks to observations performed with the Institut de Radioastronomie Millimétrique (IRAM) 30 m and the Yebes 40 m radiotelescopes and based on the extensive laboratory work reported in Penn & Curl (1971), Kaushik & Woods (1982) and Widicus et al. (2003). Prior research suggests that complex sulfur-containing species are also present in G+0.693 (Rodríguez-Almeida et al. 2021), therefore, the G+0.693 molecular cloud is a promising source to search also for cysteamine, and a careful analysis of the spectral data is needed before undertaking this task. The possible formation routes of cysteamine in the ISM are not known. Following the chemical pathways proposed by Rivilla et al. (2021b) for its O-bearing analog ethanolamine, cysteamine might be formed from S-bearing substitutes, for instance, through the radical-radical reaction between NH₂CH₂ and CH₂SH (instead of CH₂OH) on the surface of dust grains, or by sequential surface hydrogenation of HNCCS (instead of HNCCO). Unfortunately, no rotational spectroscopy of these S-bearing compounds is available, therefore we cannot search for them in the G+0.693 molecular cloud.

Although cysteamine is so important, the research of its spectroscopy is scarce. Nandi et al. (1982) studied its microwave spectrum in the 18–40 GHz frequency range and characterized two different folded structures of the molecule (also called conformational isomers, or conformers). On the other hand, Buemi (1996) used ab initio MP2/6-31G** calculations to study the stability of the different possible structures of cysteamine, and his conclusion agreed with Nandi's (Nandi et al. 1982) observations that the observed structures were also the most stable

ones. Because Buemi (1996) already stated that in these cases the choice of the theoretical method and basis set is crucial for the correct description of the conformational surface, we undertook a complete analysis using a more extended basis set that has proved to have a good accuracy in describing molecular systems governed by noncovalent interactions (Li et al. 2021). Higher-level calculations give more accurate results, thus guiding us to correctly interpret the molecular spectrum obtained in the laboratory. This will help us in turn in the search for cysteamine in the ISM. For this purpose, we decided to extend previous rotational spectroscopy (Nandi et al. 1982) and theoretical structural studies (Buemi 1996) on cysteamine to achieve a complete and accurate understanding of the conformational surface and to extend the detection and analysis of its rotational spectrum into the millimeter range.

2. Experimental setup

Cysteamine (purity of 95% and molecular weight of 77.15 g mol⁻¹) was purchased from Sigma-Aldrich and was used without any further purification. It appears as a white crystal at ambient conditions. The melting point of the molecule is 368 K, but it will decompose above temperatures of about 353 K (Mergler et al. 2011).

Two different spectrometers working in the microwave and millimeter frequency regions were used in this experiment. The spectra within the 59.6–120 GHz range were recorded by the Stark-modulated free-jet absorption millimeter-wave (FJ-AMMW) spectrometer, whose details were described previously (Calabrese et al. 2013b, 2015; Vigorito et al. 2018). The sample was kept at room temperature (300 K) while a stream of carrier gas [$P_0(\text{Ar}) = 16.5$ kPa or $P_0(\text{He}) = 25$ kPa] was flowed over it. Because the reported vapor pressure of cysteamine at 298 K is 3.22 mbar (322 Pa)¹, this results in a concentration of the sample in the carrier gas of 2% in Ar and 1.2% in He. The mixture was then expanded to about $P_b = 0.5$ Pa through a pinhole nozzle with a 0.3 mm diameter. The rotational temperature of the molecules in the jet is estimated to be 5–10 K. The estimated uncertainty for the measurements is about 50 kHz, and lines separated by more than 300 kHz are distinguishable.

Following these measurements, the rotational spectrum of cysteamine was measured using a COBRA-type pulsed supersonic-jet Fourier-transform microwave (FTMW) spectrometer upgraded with the FTMW++ set of programs (Andresen et al. 1990, 1994; Caminati et al. 2016). This spectrometer works within the 6.5–18 GHz frequency range, the estimated accuracy of frequency measurements is better than 3 kHz, and the resolution is 7 kHz. Helium was passed over the molecular sample at $T = 300$ K under a backing pressure $P_0(\text{He}) = 250$ kPa, and expanded through a pulsed valve to about 10^{-3} Pa. The rotational temperature of the sample in the supersonic expansion is about 2 K.

3. Conformational analysis

The Gaussian (Gaussian, Inc., Wallingford, CT, U.S.A.) software package (G16, revision C.01) (Frisch et al. 2016) was used to theoretically investigate cysteamine at the B3LYP-GD3(BJ)/Def2-TZVP level of calculation. The structure of the molecule is shown in Fig. 1. The three dihedral angles used to define its conformations are also given: HS-CC (φ), SC-CN (τ), and (lp)N-CC (θ), where (lp) indicates the direction of the nitrogen lone

¹ Data are given by the Hazardous Substances Data Bank (HSDB).

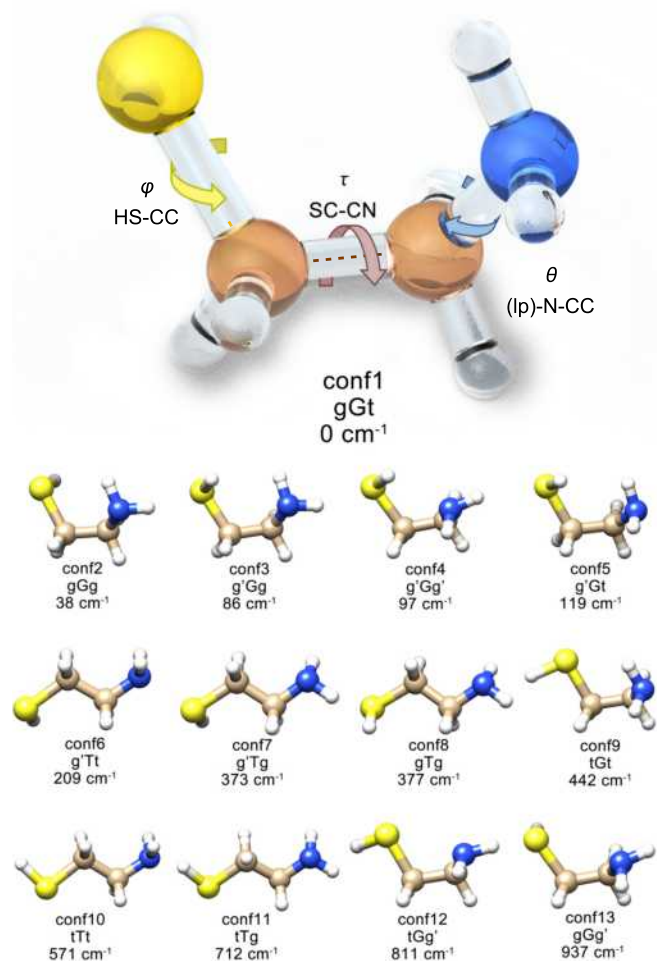


Fig. 1. Structures and zero-point corrected relative energies of the 13 conformers of cysteamine calculated at the B3LYP-GD3(BJ)/Def2TZVP level. The three dihedral angles defining the structure are marked for the most stable conformer in the upper part of the figure.

pair. For each of them, three staggered orientations are possible: *gauche* $\approx 60^\circ$, *trans* $\approx 180^\circ$, and *gauche'* $\approx 300^\circ$, which provide $3^3 = 27$ possible rotamers. Considering the values of the three dihedral angles comprehensively, we can label the rotamers using a three-letter code that describes the $\varphi\tau\theta$ values, for example, *gGt*, where $\varphi \approx 60^\circ$, $\tau \approx 60^\circ$, and $\theta \approx 180^\circ$. The central capital letter is used to identify the heavy atom skeletal arrangement, and the complete list of rotamers is given in Table 1. Except for *tTt*, the rotamers exist in specular pairs, (e.g., *gGt* and *g'G't*) thus the number of nonequivalent staggered rotamers reduces to 14. However, structural optimizations followed by frequency calculations to confirm that the structures are real minima led to only 13 stable conformations (Fig. 1), whose relative energy values are listed in Table 1. The complete set of spectroscopic constants for all conformers including rotational constants and electric dipole moment components is given in Table 2. The conformers are also numbered according to their relative energy levels, as shown in Fig. 1 and Table 1.

From these results, we can conclude that the most stable conformer is *gGt* and the five most stable conformers all possess a *gauche* skeleton of heavy atoms, allowing for an intermolecular interaction between the thiol and amino groups: both *gGt* and *gGg* conformers (conf1 and conf2) possess $\text{NH}\cdots\text{S}$ hydrogen

Table 1. Calculated electronic and zero-point-corrected relative energy values for all conformers of cysteamine (B3LYP-GD3(BJ)/Def2-TZVP).

Conformer	ΔE_e (cm^{-1})	ΔE_0 (cm^{-1})	
1	<i>gGt/g'G't</i>	0	0
2	<i>gGg/g'G'g'</i>	18	38
3	<i>g'Gg/g'G'g'</i>	55	86
4	<i>g'Gg'/gG'g</i>	79	97
5	<i>g'Gt/gG't</i>	127	119
6	<i>gTt/g'Tt</i>	249	209
7	<i>gTg/g'Tg'</i>	429	377
8	<i>gTg'/g'Tg</i>	434	373
9	<i>tGt/tG't</i>	498	442
10	<i>tTt</i>	627	571
11	<i>tTg/tTg'</i>	775	712
12	<i>tGg'/tG'g</i>	837	811
13	<i>gGg'/g'G'g</i>	1069	937
14	<i>tGg/tG'g'</i>	Not a minimum	

bonds, while the *g'Gg'* conformer (conf4) has an $\text{SH}\cdots\text{N}$ hydrogen bond and both *g'Gg* and *g'Gt* conformers (conf3 and conf5) exhibit an $\text{NH}\cdots\text{HS}$ proximity. In contrast, this type of interactions is not possible in the *trans* skeletal conformers.

It is interesting to compare these results to those found for the oxygen analog of cysteamine, 2-aminoethanol. Its conformational space has been theoretically modeled by Buemi (1996), Silva et al. (1999), and Novakovskaya & Rodnikova (2015), while Penn & Curl (1971), Kaushik & Woods (1982) and Widicus et al. (2003) studied it through microwave spectroscopy. Only one conformer has been observed in the microwave spectroscopic studies: this conformer is stabilized by an $\text{OH}\cdots\text{N}$ hydrogen bond and, following the same nomenclature as proposed in this work for cysteamine, it can be called *g'Gg'*. Thus, it does not correspond to the global minimum found for cysteamine, but rather to the structure found to be fourth in energy in the sulfur analog (conf4).

In previous experimental studies on cysteamine, (Nandi et al. 1982) two conformers were characterized. They correspond to *g'Gg* (conf3) and *g'Gg'* (conf4) in our study. Neither is the most stable conformation in our theoretical calculation, with 97 cm^{-1} and 119 cm^{-1} relative energies with respect to the global minimum *gGt* (conf1).

4. Rotational spectra

First, the FJ-AMMW spectrometer was used to perform the measurements, using argon as the carrier gas. Three conformers were observed, corresponding to conf1, conf2, and conf3 (this numbering is used from now on). Conf4 and conf5, however, were not detected despite their relative energies of 79 cm^{-1} and 127 cm^{-1} , respectively, which results in sizable calculated spectral intensities. A possible explanation for this could be that these conformers relax to lower energy conformers, which can occur when low barriers to interconversion are present. By analyzing the potential energy surface (PES) reported in Fig. 2, we can see that there are low barriers from conf4 to conf3 (293 cm^{-1}), as well as from conf5 to conf1 (471 cm^{-1}). As shown in Fig. 2, the barrier from conf4 to conf3 is only 293 cm^{-1} and the barrier from conf5 to conf1 is about 471 cm^{-1} . According to the literature, when the barrier is higher than 400 cm^{-1} , no relaxation occurs, regardless of which carrier gas is used, while for barriers

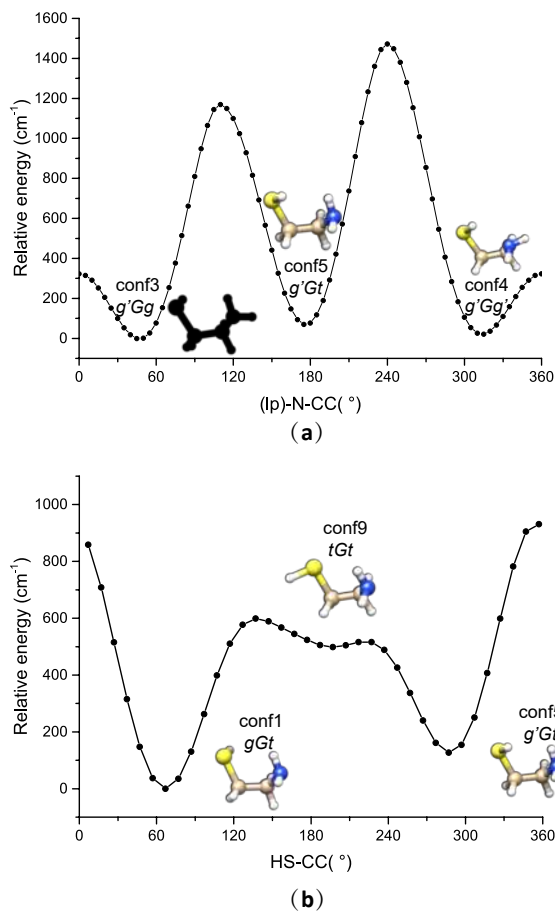


Fig. 2. 1D PES of (a) *g'G*-cysteamine and (b) *Gt*-cysteamine obtained at the B3LYP-GD3(BJ)/Def2TZVP level of calculation by scanning the dihedral angles θ ((lp)-N-CC, a) and φ (HS-CC, b) by 10° steps in the 0–360° range, while all the other parameters were freely optimized.

lower than 350 cm^{-1} , relaxation is observed in argon expansions (Ruoff et al. 1990). The difference in the relaxation processes in argon and helium expansions were described in detail by Vigorito et al. (2018) in their study of 1,2-butanediol. Based on these studies, we can conclude that while the nonobservation of conf4 in argon expansion is completely justified, the absence of conf5 is not. In any case, in a subsequent experiment, we used helium as the carrier gas in the FJ-AMMW experiment to investigate the two missing conformers. Conformer conf4 was later discovered, but conf5 remained undetectable. A more sensitive and higher-resolution FTMW spectrometer was used to identify all five low-energy conformers with *G* skeleton including conf5 (*gGt*, *gGg*, *g'Gg*, *g'Gg'*, and *g'Gt*), as well as to observe and investigate the spectral hyperfine structure due to the nuclear quadrupole coupling. Helium was employed as the carrier gas in this case.

For conf1, both μ_b R-type lines and μ_b Q-type lines were observed ($J'_{\max} = 12$, $K'_{a\max} = 5$, $K'_{c\max} = 12$). This is in agreement with the theoretical value of μ_b ($\mu_b = -1.2\text{ D}$), whereas no μ_a -type nor μ_c -type lines were found due to the low component values of the dipole moment. The experimental spectra of conf2 and conf3 appear to be similar to each other: the R- μ_a , R- μ_b and R- μ_c type lines were observed (conf2: $J'_{\max} = 11$, $K'_{a\max} = 5$, $K'_{c\max} = 10$; conf3: $J'_{\max} = 13$, $K'_{a\max} = 4$, $K'_{c\max} = 13$). In addition, μ_c Q-type lines of conf2 were also observed. For conf4 we observed only μ_a R-type transitions ($J'_{\max} = 12$, $K'_{a\max} = 7$, and $K'_{c\max} = 12$). The transitions of conf5 are of low intensity; only

the μ_c R-type and Q-type lines were detected ($J'_{\max} = 3$, $K'_{a\max} = 1$, and $K'_{c\max} = 3$).

Since ^{14}N is an atom with nuclear spin $I(^{14}\text{N}) = 1$, it can give rise to a hyperfine structure of the rotational transition due to the interaction of the ^{14}N nuclear quadrupole moment with the electric field gradient at the ^{14}N nucleus. For this reason, most of the detected lines are split ($\Delta\nu \leq 1\text{ MHz}$) into several components.

The assignments and the fits were performed using the CALPGM software, which includes the SPFIT and SPCAT programs (Pickett 1991) for fitting and predicting the spectral lines, respectively. Measured transition lines were fitted to Watson's *S*-reduced semirigid asymmetric rotor Hamiltonian (Watson 1977) in the I' representation and including the nuclear quadrupole coupling term

$$H = H_R + H_{CD} + H_Q, \quad (1)$$

where H_R is the rotational Hamiltonian containing the rotational constants A , B and C , the H_{CD} term describes the centrifugal distortion effect during the molecular rotation and H_Q includes the nuclear quadrupole coupling interaction. The results of the fitting procedure are reported in Table 2 while the experimental frequencies are available at the CDS. As indicated in the table, in the fitting we also used 51 and 75 lines from Nandi's work for conformer conf3 and conf4, respectively. The analysis of the data shows that the B3LYP-GD3(BJ)/Def2-TZVP method performs well in predicting the structures; indeed, the calculated rotational constants do not deviate much from the experimental ones; the maximum deviation being lower than 1%. The abundance of the different conformers in the jet expansion was calculated from relative intensity measurement performed with the two experimental setups and with a different carrier gas (He and Ar). The results show that in He expansion the abundance of conformers 1:2:3:4:5 is 1:0.74:0.20:0.15:0.15, which is in agreement with the calculated energy order. The same measurements performed in Ar expansion on the three observed conformers show a different ordering of abundances: 1:2:3 = 0.29:0.35:1. While it is predicted that conf1 and conf2 should have a similar abundance, that of conf3 is augmented in the Ar expansion. This result is in agreement with the nonobservation of conf4, which evidently relaxes onto conf3.

4.1. Isotopologs

Spectra for the ^{34}S isotopologs of the four most stable conformers, conf1, conf2, conf3, and conf4, were observed in natural abundance in the FTMW spectra. The spectral intensities of ^{34}S isotopologs are about 4.47% of their parent species, as a consequence of the natural abundances of the sulfur isotopes (94.99% for ^{32}S and 4.25% for ^{34}S). Also in natural abundance, all other mono-substituted isotopes of heavy atoms, two ^{13}C (1.1%) and the ^{15}N (0.4%), were detected for conf2 and conf3, which possess the most intense transitions in the 6–18 GHz region. Since the spin of ^{15}N is $1/2$, there is no splitting due to the quadrupole coupling in the rotational spectrum of this isotopolog. The spectroscopic constants of all detected isotopologs are shown in Table 3 while the experimental frequencies are available at the CDS.

4.2. Prediction for interstellar search

Based on the experimental spectroscopic parameters and the calculated values of the electric dipole moment components and energies, the simulated absorption spectra of the five most stable

Table 2. Computational and experimental spectroscopic parameters for all detected conformers of cysteamine.

	conf1 (<i>gGt</i>)		conf2 (<i>gGg</i>)		conf3 (<i>g'Gg</i>)		conf4 (<i>g'Gg'</i>)		conf5 (<i>g'Gt</i>)	
	calc.	exp.	calc.	exp.	calc.	exp.	calc.	exp.	calc.	exp.
<i>A</i> (MHz)	11895.24	11 852.9063(7) ^(a)	12 066.26	12 008.0185(8)	11969.30	11 932.433(2)	12 023.21	12 042.9(3)	11 965.26	11 944.628(2)
<i>B</i> (MHz)	3286.19	3310.6341(6)	3337.32	3363.5781(3)	3375.38	3394.9980(3)	3354.63	3352.2284(9)	3277.90	3292.205(2)
<i>C</i> (MHz)	2850.69	2866.4712(4)	2882.36	2898.8592(3)	2861.51	2877.8302(3)	2878.65	2881.9906(7)	2812.82	2827.008(3)
<i>D_J</i> (kHz)	2.11	2.13(1)	2.13	2.181(5)	2.32	2.347(3)	2.19	2.201(5)	2.16	[0] ^(b)
<i>D_{JK}</i> (kHz)	-10.20	-9.95(6)	-10.06	-10.00(4)	-10.74	-11.2(1)	-11.81	-11.83(5)	-10.88	[0]
<i>D_K</i> (kHz)	40.86	39.4(1)	40.22	39.6(1)	41.67	42.9(2)	44.74	[0]	45.43	[0]
<i>d₁</i> (kHz)	-0.50	-0.496(6)	-0.52	-0.535(3)	-0.61	-0.616(3)	-0.56	-0.547(8)	-0.54	[0]
<i>d₂</i> (kHz)	-0.03	-0.030(3)	-0.03	-0.038(1)	-0.05	-0.043(3)	-0.04	-0.025(6)	-0.04	[0]
1.5 χ_{aa} (MHz)	-4.32	-3.873(3)	3.19	2.609(3)	3.34	2.614(3)	-2.87	-2.443(8)	-5.51	-4.77(1)
0.25($\chi_{bb} - \chi_{cc}$) (MHz)	0.51	0.481(1)	1.87	1.6767(9)	1.94	1.703(1)	-0.69	-0.518(3)	0.42	0.422(3)
σ ^(c) (kHz)		38		40		32		35		6
<i>N</i> ^(d)		163 (0/24/139)		304 (0/38/266)		191 (51/24/116)		141 (75/16/49)		16 (0/16/0)
μ_{al} (D)	0.00	n ^(e)	0.98	y	1.59	1.6(1) ^(f) /y	2.92	2.68(1)/y	0.29	n
μ_{bl} (D)	1.22	y	-0.83	y	0.32	0.0(2)/y	0.84	0.88(2)/n	0.44	n
μ_{cl} (D)	0.27	n	1.66	y	0.49	0.6(2)/y	0.35	0.37(5)/n	1.25	y

Notes. ^(a)Standard error in parentheses in the units of the last digit. ^(b)Values in brackets are fixed to 0. ^(c)Rms deviation of the fit. ^(d)Number of transitions in the fit, in parentheses, the number of lines from Nandi's work are shown on the left, the number of lines measured by the FTMW spectrometer is shown in the middle, and the number of lines measured by the FJAMMW spectrometer is shown on the right. ^(e)y/n denotes that such transitions type have/have not been observed. ^(f)Data from Nandi et. al. (Nandi et al. 1982).

Table 3. Experimental spectroscopic parameters (MHz) for the observed isotopologs of cysteamine.

conf1	<i>A</i>	<i>B</i>	<i>C</i>	σ ^(a)	<i>N</i> ^(b)
³⁴ S	11810.420(2)	3229.8803(6)	2803.3291(9)	0.004	16
conf2	<i>A</i>	<i>B</i>	<i>C</i>	σ ^(a)	<i>N</i> ^(b)
³⁴ S	11965.455(2)	3281.2728(7)	2835.1331(7)	0.003	25
¹³ C1	11755.412(2)	3361.692(1)	2885.540(1)	0.004	12
¹³ C2	11899.745(2)	3325.578(1)	2868.097(1)	0.004	14
¹⁵ N	11850.210(5)	3295.482(2)	2840.260(2)	0.0003	4
conf3	<i>A</i>	<i>B</i>	<i>C</i>	σ ^(a)	<i>N</i> ^(b)
³⁴ S	11895.508(3)	3309.5697(8)	2814.5395(7)	0.003	20
¹³ C1	11680.5(7)	3393.005(1)	2864.5347(9)	0.002	12
¹³ C2	11827.0(8)	3356.308(1)	2847.1365(9)	0.003	10
¹⁵ N	11772(2)	3326.991(2)	2820.678(1)	0.0001	4
conf4	<i>A</i>	<i>B</i>	<i>C</i>	σ ^(a)	<i>N</i> ^(b)
³⁴ S	12001.8(9)	3267.615(1)	2817.3405(7)	0.007	12

Notes. Quartic centrifugal distortion and nuclear quadrupole coupling constants are fixed to the values determined for the parent species (Table 2). ^(a)Rms deviation of the fit. ^(b)Number of transitions in the fit.

conformers at four different temperatures were calculated and are shown in Fig 3. It is interesting to note how different the spectra are at different temperatures: (i) at $T = 10$ K, conf1 and conf2 are responsible for the dominating features in the spectrum. (ii) At $T = 50$ K, conf1 and conf2 are still the brightest features in the whole frequency range, but conf3 and conf4 have a comparable intensity in the low-frequency range. (iii) At $T = 100$ K, conf3 and conf4 dominate at low frequencies, while conf2 and conf4 dominate in the high-frequency region. (iv) At $T = 300$ K, conf4 and conf3 conformers have the most intense lines in the spectrum. This demonstrates that a comprehensive understanding of the conformational space is necessary to target the correct transitions at different temperatures and in different frequency ranges.

5. Interstellar search toward the G+0.693–0.027 molecular cloud

We have searched for the different conformers of cysteamine toward the G+0.693-0.027 molecular cloud, where the cysteamine O-bearing analog, ethanolamine ($\text{NH}_2\text{CH}_2\text{CH}_2\text{OH}$) has recently been detected (Rivilla et al. 2021b), and where several relatively complex S-bearing molecules, such as HCOSH, CH_3SH , and $\text{CH}_3\text{CH}_2\text{SH}$ have also been found (Rodríguez-Almeida et al. 2021).

The conformers were modeled as independent species, without taking into account their zeropoint energy, as was done for other species such as imines, for which both the low- and high-energy conformers were detected toward this molecular cloud (Rivilla et al. 2019). Moreover, from the theoretical point of view, this approach is preferred because the calculated relative energies (including the zeropoint corrections) are very sensitive to the theoretical method used (Calabrese et al. 2013a).

We used a sensitive unbiased spectral survey performed with the Yebes 40 m (Guadalajara, Spain) and the IRAM 30 m (Granada, Spain) telescopes. The observations, using position-switching mode, were centered at $\alpha(\text{J2000.0}) = 17^{\text{h}}47^{\text{m}}22^{\text{s}}$, $\delta(\text{J2000.0}) = -28^{\circ}21'27''$. The Yebes 40 m observations covered a total spectral range from 31.075 to 50.424 GHz. The noise of the spectra depends on the frequency range, reaching values in antenna temperature (T_A^*) as low as 1.0 mK, while in some intervals, it increases up to 4.0 mK. The IRAM 30 m observations cover the range 71.770–116.720 GHz. The noise of the spectra (in T_A^*) is 1.3–2.8 mK in the range 71–90 GHz, 1.5–5.8 mK in the range 90–115 GHz, and ~ 10 mK in the range 115–116 GHz. More detailed information of the observational survey is presented in Rivilla et al. (2021b).

We implemented the spectroscopy presented in this work into the MADCUBA package² (version 26/07/2021; Martín et al. 2019). The spectral line identification and modeling (SLIM) tool of MADCUBA uses the molecular databases of the Cologne

² Madrid Data Cube Analysis on ImageJ is a software developed at the Center of Astrobiology (CAB) in Madrid; <http://cab.inta-csic.es/madcuba/Portada.html>

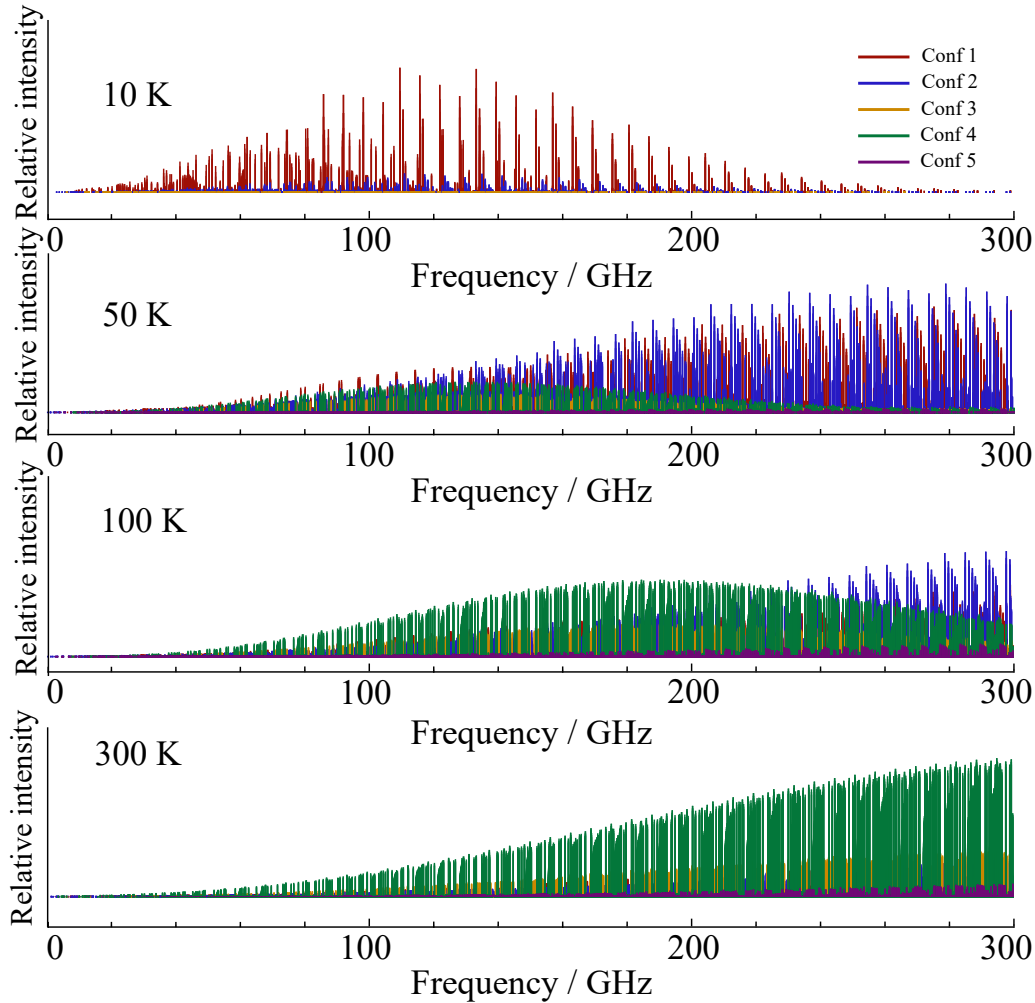


Fig. 3. Simulated spectra of the five observed conformers of cysteamine (conf1, conf2, conf3, conf4, and conf5) at $T = 10, 50, 100,$ and 300 K using SPCAT program taking into account the zeropoint-corrected relative energies and dipole moment component values (B3LYP-GD3(BJ)/Def2TZVP).

Database for Molecular Spectroscopy (CDMS; Endres et al. 2016) and the Jet Propulsion Laboratory (JPL; Pickett et al. 1998) to generate synthetic spectra under the assumption of local thermodynamic equilibrium (LTE). We implemented into SLIM the spectroscopy of the different conformers of cysteamine presented in this work. We generated their synthetic LTE spectra, which were compared with the observed spectrum. To evaluate whether the transitions are blended with emission from other species, we also considered the LTE model that predicts the total contribution of the more than 120 species identified so far toward G+0.693-0.027 (e.g., Requena-Torres et al. 2008; Zeng et al. 2018; Rivilla et al. 2019, 2020, 2021a,b; Jiménez-Serra et al. 2020).

We simulated the LTE spectra of the cysteamine isomers using the physical parameters found for ethanolamine by Rivilla et al. (2021b), which are excitation temperature $T_{\text{ex}} = 9.7$ K, line width of $FWHM = 15$ km s $^{-1}$, and $v_{\text{LSR}} = 68.4$ km s $^{-1}$. None of the cysteamine conformers were clearly detected in the observed data. In most cases, the cysteamine transitions appear to be strongly blended with brighter lines of abundant species. As an example, we show in the left panel of Fig. 4 the brightest spectral feature predicted by the LTE model of the lowest energy conformer of cysteamine, gGt , which is composed by six blended transitions at 86.05–86.06 GHz (4_4-3_3 transitions, $E_{\text{up}} = 8.02$ K). These transitions are heavily contaminated by the 1–0 rotational

transition of HC 15 N. Thus, to compute the upper limit of the different conformers of cysteamine, we searched for the brightest predicted spectral features that are not blended with emission from other molecules. In the case of gGt -cysteamine, we used a spectral feature composed of three transitions at 94.124 GHz ($E_{\text{up}} = 14.5$ K), which is shown in the right panel of Fig. 4. Using MADCUBA, we determined the upper limit of the column density using the 3σ value of the integrated intensity (see details in Martín et al. 2019). The derived upper limits for the five conformers and the information of the transitions we used are summarized in Table 4. The lowest energy conformer, gGt , has a column density of $N < 1.7 \times 10^{13}$ cm $^{-2}$, which translates into a molecular abundance with respect to molecular hydrogen of $< 1.3 \times 10^{-10}$, using $N_{\text{H}_2} = 1.4 \times 10^{23}$ cm $^{-2}$ (from Martín et al. 2008). For the other conformers, we found molecular abundances of $< 0.3-1.6 \times 10^{-10}$ (Table 4).

In the last column of Table 4 we compare the molecular column density of the oxygen-substitute of cysteamine, ethanolamine (NH $_2$ CH $_2$ CH $_2$ OH; from Rivilla et al. 2021b), with the upper limits derived for the cysteamine conformers. The ethanolamine/cysteamine ratio is > 0.8 for the lowest energy conformer, while for the other, the ratio ranges between > 0.9 and > 5.3 . These ratios indicate that the molecular abundance of cysteamine is (at most) of the same order or lower than that of its O-substitute ethanolamine in the G+0.693-0.027 molecular

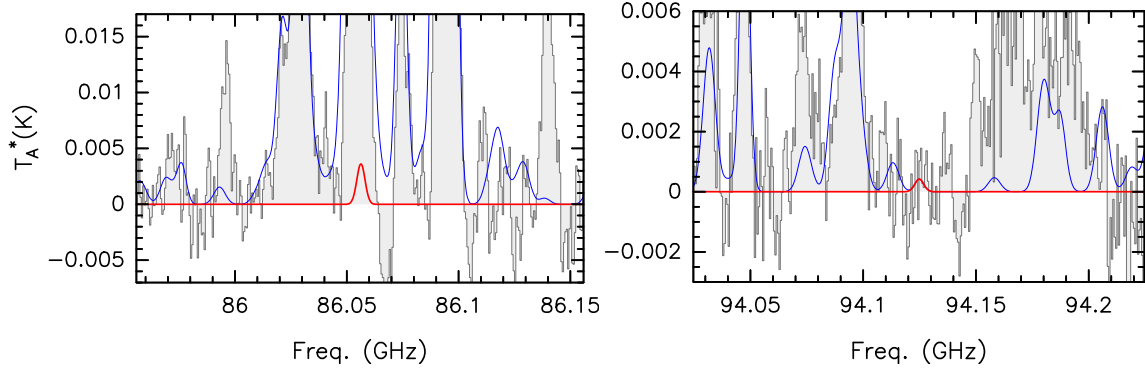


Fig. 4. Selected transitions of the *gGt* conformer of cysteamine in the spectral survey toward the G+0.693-0.027 molecular cloud. *Left panel:* brightest spectral feature of *gGt*-cysteamine, composed of six blended transitions at 86.05–86.06 GHz (4_4-3_3 , $E_{10} = 3.89$ cm $^{-1}$), predicted by the LTE spectrum obtained considering the upper limit of the column density (see Table 4). These *gGt*-cysteamine transitions appear heavily blended with a much brighter line produced by $\text{HC}^{15}\text{N}(1-0)$ at 86.05496 GHz. *Right panel:* brightest predicted spectral feature of *gGt*-cysteamine (composed by three transitions at 94.124 GHz; $E_{10} = 6.93$ cm $^{-1}$; Table 4) that is not blended with emission from other molecules. We used these transitions to compute the upper limit for the column density of *gGt*-cysteamine (Table 4). In both panels, the gray histogram shows the observed spectrum, the blue curve shows the contribution of all the molecules previously identified in the molecular cloud G+0.693-0.027, and red plots the LTE spectrum of the *gGt* conformer of cysteamine obtained with the upper limit for its column density (Table 4).

Table 4. Upper limits for the molecular column density and abundances with respect to H_2 of different conformers of cysteamine derived toward the G+0.693-0.027 molecular cloud.

Conformer	N ($\times 10^{13}$ cm $^{-2}$) ^(a)	Abundance ^(b) ($\times 10^{-10}$)	Transition ^(c)	Frequency (GHz) ^(c)	E_{up} (K)	E_{10} (K)	$N_{\text{NH}_2\text{CH}_2\text{CH}_2\text{OH}}/N$
<i>gGt</i>	<1.7	<1.3	$8_{3,5}^7-7_{2,6}^6$	94.124644	14.5	10.0	>0.8
			$8_{3,5}^8-7_{2,6}^7$	94.124663	14.5	10.0	
			$8_{3,5}^8-7_{2,6}^7$	94.124716	14.5	10.0	
<i>gGg</i>	<0.5	<0.4	$4_{4,0}^4-3_{3,0}^3$	87.184483	9.8	5.6	>3.1
			$4_{4,0}^3-3_{3,0}^2$	87.184540	9.8	5.6	
			$4_{4,0}^5-3_{3,0}^4$	87.184583	9.8	5.6	
			$4_{4,1}^4-3_{3,1}^3$	87.184920	9.8	5.6	
			$4_{4,1}^3-3_{3,1}^2$	87.184979	9.8	5.6	
			$4_{4,1}^2-3_{3,1}^1$	87.185022	9.8	5.6	
<i>g'Gg</i>	<1.6	<1.2	$6_{1,6}^7-5_{1,5}^6$	35.918699	6.5	4.7	>0.9
<i>g'Gg'</i>	<0.3	<0.2	$7_{1,6}^7-6_{1,5}^6$	45.008702	9.1	6.9	>5.3
			$7_{1,6}^6-6_{1,5}^5$	45.008734	9.1	6.9	
			$7_{1,6}^8-6_{1,5}^7$	45.008734	9.1	6.9	
<i>g'Gt</i>	<1.4	<1.1	$8_{3,5}^7-7_{2,5}^6$	92.165413	14.4	10.0	>1.0
			$8_{3,5}^9-7_{2,5}^8$	92.165470	14.4	10.0	
			$8_{3,5}^8-7_{2,5}^7$	92.165763	14.4	10.0	

Notes. We include the molecular transitions used to compute the upper limits, and the relative molecular ratio of ethanolamine ($\text{NH}_2\text{CH}_2\text{CH}_2\text{OH}$) with respect to each cysteamine conformer. ^(a)Upper limits derived assuming $T_{\text{ex}} = 9.7$ K, $FWHM = 15$ km s $^{-1}$, and $v_{\text{LSR}} = 68.4$ km s $^{-1}$, obtained from the fit of ethanolamine ($\text{NH}_2\text{CH}_2\text{CH}_2\text{OH}$; Rivilla et al. 2021b). ^(b)We adopted $N_{\text{H}_2} = 1.4 \times 10^{23}$ cm $^{-2}$ from Martín et al. (2008). ^(c)Molecular transitions used to derive the upper limits. The notion used is J_{K_a, K_c}^F .

cloud. This result is in good agreement with the ratios previously found between several alcohols (-OH) and thiols (-SH) in this cloud which are reported in Table 5. Rodríguez-Almeida et al. (2021) found that the relative ratios of the pairs $\text{CH}_3\text{OH}/\text{CH}_3\text{SH}$, $\text{t-HCOOH}/\text{t-HCOOH}$, $\text{CH}_3\text{CH}_2\text{OH}/\text{CH}_3\text{CH}_2\text{SH}$ are ~ 13 – 23 , indicating that the S-bearing substitutes are at least one order of magnitude less abundant than the O-bearing substitutes. This ratio is similar to the ratio of the cosmic abundances of oxygen and sulfur (~ 30 ; Grevesse & Sauval 1998), which suggests that the cosmic availability of both elements might be the dominant factor behind the observed difference between O- and S-bearing molecular counterparts toward G+0.693-0.027. If this is true for all species, the detection of S-bearing counterparts

of O-bearing COMs is highly challenging. For the case of cysteamine, it would require much deeper integration times (by two orders of magnitude) using the current telescopes, which is almost impossible. A new generation of facilities, such as the next-generation VLA (ngVLA), might help to enable this type of detection in the future.

6. Summary and conclusions

The conformational space of cysteamine (the sulfur analog of ethanolamine) and the measurement and analysis of its rotational spectra in the 6–18 and 59.6–120 GHz are reported. The five most stable conformers all with a *gauche* skeleton were detected

Table 5. Molecular ratios of alcohols and thiols toward the molecular cloud G+0.693-0.027.

Molecular family	OH/SH	Reference
CH ₃ –	23 ± 3	1
HCO– ^(a)	13 ± 4	1
CH ₃ CH ₂ –	15 ± 7	1
NH ₂ CH ₂ CH ₂ –	>0.8	2 and this work

Notes. ^(a)We considered the column densities of t-HCOOH and t-HCOSH.

References. 1: Rodríguez-Almeida et al. (2021); 2: Rivilla et al. (2021b).

and characterized by rotational spectroscopy, while no *trans* conformers were observed because their relative energies are higher. *gGt* conformer with NH...S hydrogen bond was determined as the global minimum. The *g'Gg* and *g'Gt* conformers have NH...HS proximity, and their binding energies are comparable to those of the SH...N hydrogen-bonded conformations.

The spectra were analyzed using the CALPGM software (Pickett 1991); with respect to previous work (Nandi et al. 1982), three more low-energy conformers were characterized. For four of them, the rotational constants and the quartic centrifugal distortion constants were determined, while for conf5, only the rotational constants were determined because only a few lines were detected: due to the low intensity of its spectrum. The hyperfine structure of the rotational spectra was observed and analyzed, and nuclear quadrupole coupling constants for all the five observed conformers were obtained for the first time. Moreover, the rotational spectra of ten isotopologs observed in natural abundance are reported. The comparison of the obtained rotational constants to the theoretical calculations can be used to test the accuracy of the theoretical model in predicting molecular structures.

The experimentally determined spectroscopic parameters were then used to predict the rotational spectrum of cysteamine at various temperatures. Considering the different frequency zones, the spectra show different prominent features at the variation of the temperature, demonstrating that for flexible molecules such as cysteamine, it is important to achieve a complete spectral characterization of the low-energy conformations in order to target the correct transitions in an astronomical search.

Based on the predicted spectra, a search of the different conformers of cysteamine was performed toward the G+0.693-0.027 molecular cloud, where its O-bearing analog (ethanolamine) was detected. The search was unfruitful, and no transitions of cysteamine were found. We computed the upper limit of the ratio of ethanolamine to cysteamine, which is >0.8–5.3, in agreement with the OH/SH ratios found previously in another molecule.

Acknowledgements. We acknowledge the CINECA award under the ISCRA initiative, for the availability of high-performance computing resources and support. D.L. and W.S. thank the China Scholarship Council (CSC) for financial support. This work was supported by the Italian MIUR (Attività Base di Ricerca) and the University of Bologna (Ricerca Fondamentale Orientata). V.M.R. has received funding from the Comunidad de Madrid through the Atracción de Talento Investigador (Doctores con experiencia) Grant (COOL: Cosmic Origins Of Life; 2019-T1/TIC-15379). The paper is published with the contribution of the Department of Excellence program financed by the Ministry of Education, University and Research (MIUR, L. 232 del 01/12/2016).

References

Altwegg, K., Balsiger, H., Berthelier, J.-J., et al. 2017, *MNRAS*, **469**, S130
Andresen, U., Dreizler, H., Grabow, J.-U., & Stahl, W. 1990, *Rev. Sci. Instrum.*, **61**, 3694

Andresen, U., Dreizler, H., Kretschmer, U., Stahl, W., & Thomsen, C. 1994, *Fresenius' J. Anal. Chem.*, **349**, 272
Bossa, J. B., Theule, P., Duvernay, F., & Chiavassa, T. 2009, *ApJ*, **707**, 1524
Buemi, G. 1996, *Int. J. Quant. Chem.*, **59**, 227
Calabrese, C., Maris, A., Evangelisti, L., Caminati, W., & Melandri, S. 2013a, *Chem. Phys. Chem.*, **14**, 1943
Calabrese, C., Maris, A., Evangelisti, L., et al. 2013b, *J. Phys. Chem. A*, **117**, 13712
Calabrese, C., Vigorito, A., Maris, A., et al. 2015, *J. Phys. Chem. A*, **119**, 11674
Caminati, W., Evangelisti, L., Feng, G., et al. 2016, *PCCP*, **18**, 17851
Charnley, S. B. 1997, *ApJ*, **481**, 396
Charnley, S. B., Ehrenfreund, P., & Kuan, Y. J. 2001, *Spectrochim. Acta A Mol. Biomol. Spectr.*, **57**, 685
Courmier, D., Gardebien, F., Minot, C., & St-Amant, A. 2005, *Chem. Phys. Lett.*, **405**, 357
Duvernay, F., Dufaut, V., Danger, G., et al. 2010, *A&A*, **523**, A79
Endres, C. P., Schlemmer, S., Schilke, P., Stutzki, J., & Müller, H. S. P. 2016, *J. Mol. Spectr.*, **327**, 95
Frisch, M. J., Trucks, G. W., Schlegel, H. B., et al. 2016, *Gaussian~16 Revision B.01* (Wallingford CT: Gaussian Inc)
Gibb, E., Nummelin, A., Irvine, W. M., Whittet, D., & Bergman, P. 2000, *ApJ*, **545**, 309
Goicoechea, J. R., Aguado, A., Cuadrado, S., et al. 2021, *A&A*, **647**, A10
Grevesse, N., & Sauval, A. J. 1998, *Space Sci. Rev.*, **85**, 161
Hatchell, J., Thompson, M. A., Millar, T. J., & Macdonald, G. H. 1998, *A&A*, **338**, 713
Jiménez-Serra, I., Martín-Pintado, J., Rivilla, V. M., et al. 2020, *Astrobiology*, **20**, 1048
Joseph, C. L., Snow Jr, T. P., Seab, C. G., & Crutcher, R. M. 1986, *ApJ*, **309**, 771
Kaushik, V. K., & Woods, R. C. 1982, *Z. Phys. Chem.*, **132**, 117
Kolesniková, L., Tercero, B., Cernicharo, J., et al. 2014, *ApJ*, **784**, L7
Laas, J. C., & Caselli, P. 2019, *A&A*, **624**, A108
Lada, E. A., Bally, J., & Stark, A. A. 1991, *ApJ*, **368**, 432
Li, W., Usabiaga, I., Calabrese, C., et al. 2021, *PCCP*, **23**, 9121
Linke, R., Frerking, M., & Thaddeus, P. 1979, *ApJ*, **234**, L139
Majumdar, L., Gratier, P., Vidal, T., et al. 2016, *MNRAS*, **458**, 1859
Maris, A., Calabrese, C., Favero, L. B., et al. 2019, *ACS Earth Space Chem.*, **3**, 1537
Martín, S., Requena-Torres, M. A., Martín-Pintado, J., & Mauersberger, R. 2008, *ApJ*, **678**, 245
Martín, S., Martín-Pintado, J., Blanco-Sánchez, C., et al. 2019, *A&A*, **631**, A159
Mergler, Y., Rumley-Van Gorp, R., Brassier, P., De Koning, M., & Goetheer, E. 2011, *Energy Procedia*, **4**, 259
Motiyenko, R. A., Belloche, A., Garrod, R. T., et al. 2020, *A&A*, **642**, A29
Müller, H. S., Belloche, A., Xu, L.-H., et al. 2016, *A&A*, **587**, A92
Nandi, R., Boland, M. F., & Harmony, M. D. 1982, *J. Mol. Spectr.*, **92**, 419
Novakovskaya, Y. V., & Rodnikova, M. N. 2015, *Struc. Chem.*, **26**, 177
Oya, Y., López-Sepulcre, A., Sakai, N., et al. 2019, *ApJ*, **881**, 112
Penn, R. E., & Curl, R. F. 1971, *J. Chem. Phys.*, **55**, 651
Pickett, H. M. 1991, *J. Mol. Spectr.*, **148**, 371
Pickett, H. M., Poynter, R. L., Cohen, E. A., et al. 1998, *J. Quant. Spectr. Rad. Transf.*, **60**, 883
Plume, R., Jaffe, D., Evans II, N. J., Martín-Pintado, J., & Gomez-Gonzalez, J. 1997, *ApJ*, **476**, 730
Remijan, A., Xue, C., Margulès, L., et al. 2022, *A&A*, **658**, A85
Requena-Torres, M., Martín-Pintado, J., Martín, S., & Morris, M. 2008, *ApJ*, **672**, 352
Rivilla, V., Martín-Pintado, J., Jiménez-Serra, I., et al. 2019, *MNRAS*, **483**, L114
Rivilla, V. M., Martín-Pintado, J., Jiménez-Serra, I., et al. 2020, *ApJ*, **899**, L28
Rivilla, V. M., Jiménez-Serra, I., García de la Concepción, J., et al. 2021a, *MNRAS*, **506**, L79
Rivilla, V. M., Jiménez-Serra, I., Martín-Pintado, J., et al. 2021b, *PNAS*, **118**, e2101314118
Rodríguez-Almeida, L. F., Jiménez-Serra, I., Rivilla, V. M., et al. 2021, *ApJ*, **912**, L11
Ruoff, R., Klots, T., Emilsson, T., & Gutowsky, H. 1990, *J. Chem. Phys.*, **93**, 3142
Savage, B. D., & Sembach, K. R. 1996, *A&ARv*, **34**, 279
Silva, C. F., Duarte, M. L. T., & Fausto, R. 1999, *J. Mol. Struct.*, **482**, 591
Vigorito, A., Calabrese, C., Melandri, S., et al. 2018, *A&A*, **619**, A140
Wakelam, V., Hersant, F., & Herpin, F. 2011, *A&A*, **529**, A112
Watson, J. 1977, in *Vibrational Spectroscopy and Structure*; Durig, JR (Amsterdam: Elsevier)
Widicus, S. L., Drouin, B. J., Dyl, K. A., & Blake, G. A. 2003, *J. Mol. Spectr.*, **217**, 278
Zeng, S., Jiménez-Serra, I., Rivilla, V., et al. 2018, *MNRAS*, **478**, 2962